Contents

1
Introduction

This thesis investigates a numerical approximation method put forth by Baxter in 1978 [1–3] based on the corner transfer matrix formulation of the partition function for two-dimensional classical lattice models.

The method rose to prominence in 1996, under the name *corner transfer matrix renormalization group* (CTMRG), when Nishino showed [4] that in the thermodynamic limit, it is equivalent to the hugely successful density matrix renormalization group (DMRG) method for one-dimensional quantum systems [5], discovered a few years earlier by White.

The error in the CTMRG method comes from the fact that the corner transfer matrices, whose dimension diverges exponentially in the lattice size, have to be truncated at a maximum dimension m in order to make numerical manipulation possible. This finite *bond dimension* m (also denoted by χ or D in the literature) introduces finite-size effects, comparable to those observed for systems that are finite in one or more spatial dimensions. This was already realized by Nishino [6].

The main objective of this thesis is to study how *finite bond dimension scaling* may be performed with the CTMRG method.

Before the structure of this thesis is laid out, I will first make some general remarks on statistical mechanics and phase transitions, and on how the CTMRG method relates to the class of newer methods for simulating many-body systems that grew out of White's breakthrough, known as *tensor network algorithms*.

1.1 Statistical mechanics and phase transitions

Statistical mechanics is concerned with describing the average properties of systems consisting of many particles. Examples of such systems are the atoms

making up a bar magnet, the water molecules in a glass of water, or virtually any other instance of matter around us.

Matter can arrange itself in various structures with fundamentally different properties. We call these distinct states of matter *phases*. When matter changes from one phase to another, we say it undergoes a phase transition.

Physics has made great strides in understanding these transitions. The complete history of the field is beyond the scope of this introduction and this thesis, but the reader may wish to consult [7, 8] to get an idea.

Only as late as 1936, the occurrence of a phase transition within the framework of statistical physics was established by R. Peierls [9]. He showed that the two-dimensional Ising model has a non-zero magnetization for sufficiently low temperatures. Since for high enough temperatures the Ising model loses its magnetization, it follows that there must be phase transition in between.

The effort to understand the Ising model culminated with Onsager's exact solution in 1944 [10], which rigorously established a sharp transition point in the thermodynamic limit. In the years that followed, more models were exactly solved. Examples are the spherical model [11] (1952), ice-type models [12] (1967) and the eight-vertex model [13] (1971). A pedagogical treatment of these and other models can be found in [14].

In the meantime, various approximation methods were developed. With rapidly improving computers, the method of statistical sampling (Monte Carlo) became one of the most prominent and its significance has not waned. Other methods are, among others, series expansions and variational approximations. A variational approximation put forth by Kramers and Wannier (1941) [15] was later seen to be equivalent to Baxter's corner transfer matrix method with $m = 1$.

1.1.1 Universality

One may question the relevance of studying very simple models such as the Ising model. As it turns out, systems that are at first sight vastly different may show qualitatively similar behaviour near a phase transition. For example, exponents that characterize the divergence of quantities near a transition are conjectured to be independent on microscopic details of the interactions between particles, but instead fall into distinct *universality classes* [16, 17]. Thus, studying the very simplest model may yield universal results.

1.2 Baxter's method as a precursor to tensor network methods

Baxter showed that the optimal truncation of corner transfer matrices corresponds, in the thermodynamic limit, to a variational optimization of the row-to-row transfer matrix within a certain subspace, now known as the subspace of *matrix product states* (MPSs) [2, 18].

After the success of White's DMRG, which, as Nishino pointed out, is equivalent to Baxter's method, the underlying matrix-product structure was rediscovered in the context of one-dimensional quantum systems by Östlund and Rommer [19, 20].

It is historically significant but little known that Nightingale, in a footnote of a 1986 paper [21], already made the remark that "The generalization [of Baxter's method] to quantum mechanical systems is straightforward."

After Östlund and Rommer, it was realized that reformulating White's algorithm directly in terms of matrix product states provided the explanation of the algorithm's shortcomings around phase transitions. An MPS-ansatz fundamentally limits the entropy of the ground state approximation and since the entropy diverges at a conformally invariant critical point [22], DMRG gives inaccurate results.

This gave rise to other ansätze, formulated in the language of tensor networks [23], specifically designed to represent states with a certain amount of entropy. Examples are multi-scale entanglement renormalization ansatz (MERA) for critical one-dimensional quantum systems [24] and projected entangled-pair states (PEPS) [25] for two-dimensional quantum systems.

Other tensor network algorithms, such as infinite time-evolving block decimation [26] in one dimension and iPEPS (infinite PEPS) [27] in two dimensions made it possible to directly approximate quantum systems in the thermodynamic limit.

iTEBD was used to study finite bond dimension scaling (under the slightly different name of *finite-entropy scaling*) [28]. Some theoretical predictions were later made in [29].

The goal of this thesis is twofold: (i) investigate how finite bond dimension scaling works in the CTMRG algorithm for classical systems, where we can directly compare it with finite-size scaling, and (ii) investigate how it compares to different numerical approaches, such as iTEBD or Monte Carlo.

For (i), I have studied the Ising model, for which all results may be checked against the exact solution. For (ii), I have studied the clock model with $q =$

$\{5, 6\}$ states, which is regarded as difficult numerically and subject to some controverse.

1.3 Structure of this thesis

It is in the mostly quantum-oriented research field sketched above that the work for this thesis was done. Therefore, I have chosen to begin by introducing White's algorithm in its original description (chapter two), before making the connection to two-dimensional classical lattices and properly introducing the corner transfer matrix formulation (chapter three).

In chapter four, the concepts of critical behaviour and finite-size scaling are introduced and in chapter five these concepts are connected to the work already done on finite bond dimension (or finite-entropy) scaling.

Technical details and convergence behaviour of the CTMRG algorithm are reported in chapter six. It is found that the values of observables may be accurately extrapolated in the chosen convergence criterion of the algoritm.

Results for the Ising model are presented and analyzed in chapter seven. With finite-m simulations, it is much easier to reach large system sizes, but thermodynamic quantities do not grow smoothly as a function of the bond dimension, as a result of the underlying spectrum of the corner transfer matrix.

Quantities calculated with finite-size simulations do not suffer this unsmooth behaviour. Results for both methods are comparable, but it is plausible that finite-size data turns out to be more accurate when corrections to scaling are included.

A numerical analysis of the clock model with $q = \{5, 6\}$ states is given in chapter eight. The model has a low-temperature ordered phase, a massless phase and a high-temperature disordered phase. The transition temperatures T_1 and T_2 are located by extrapolating the positions of pseudocritical temperatures, assuming the transitions are of the Kosterlitz-Thouless type. I find slightly contradictory results, based on exact results in a related formulation of the model, but argue it is plausible that this is due to finite-size effects.

2
Numerical results for the Ising model

We present numerical results of finite-m and finite-size scaling within the CTMRG method on the Ising model.

With finite-m simulations, it is much easier to reach large system sizes, but thermodynamic quantities do not grow smoothly as a function of m, as a result of the underlying spectrum of the corner transfer matrix. This makes it harder to fit the basic power law divergences. Defining the correlation length in terms of the classical analogue to the entanglement entropy mitigates this effect somewhat.

Quantities calculated with finite-size simulations do not suffer this unsmooth behaviour. Results for both methods are comparable, but it is plausible that finite-size data turns out to be more accurate when corrections to scaling are included.

Apart from thermodynamic quantities, we also accurately compute the central charge of the critical point with both methods. Additionally, we verify the relation $\xi(m) \propto m^{\kappa}$ at the critical point, although the value of κ found in this work is slightly lower than predicted in the literature.

2.1 At the critical point

2.1.1 Existence of two length scales

First, we reproduce the results presented in [6] to validate the assumption that at the critical point, the only relevant length scales are the system size N and the length scale associated to a finite dimension m of the corner transfer matrix $\xi(m)$. Here, we assume that $\xi(m)$ is given by the correlation length at the critical point, see ??.

The order parameter[1] should obey the following scaling relation at the

[1] It is worth stressing that the order parameter and the magnetization per site are used inter-

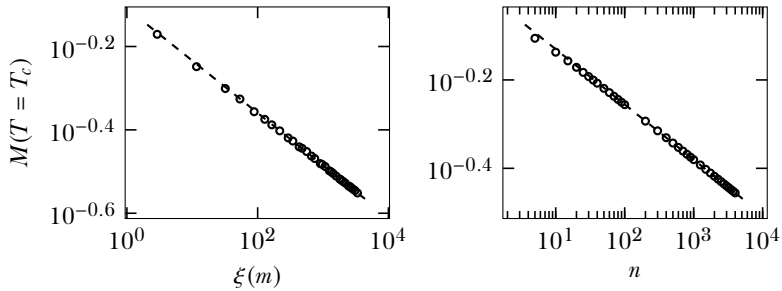

Figure 2.1: Left panel: fit to the relation in Eq. 2.1, yielding $\frac{\beta}{\nu} \approx 0.125(5)$. The data points are obtained from simulations with $m = 2, 4, \ldots, 64$. The smallest 10 values of m have not been used for fitting, to diminish correction terms to the basic scaling law. Right panel: fit to conventional finite-size scaling law given in Eq. 2.2, fitted with $n = 1500, 1750, \ldots, 4000$, calculated with a truncation error no larger than 10^{-7}, yielding $\beta/\nu \approx 0.1249$.

critical temperature

$$M(T = T_c, m) \propto \xi(T = T_c, m)^{-\beta/\nu}. \tag{2.1}$$

The left panel of Fig. 2.1 shows that this scaling relation holds. The fit yields $\frac{\beta}{\nu} \approx 0.125(5)$, close to the true value of $\frac{1}{8}$.

The right panel shows the conventional finite-size scaling relation

$$M(T = T_c, N) \propto N^{-\beta/\nu}, \tag{2.2}$$

yielding $\beta/\nu \approx 0.1249(1)$.

The correlation length $\xi(m)$ shows characteristic half-moon patterns on a log-log scale, stemming from the smeared-out stepwise pattern in the corner transfer matrix spectrum (see ??). This makes the data harder to interpret, since the effect of increasing m depends on how much of the spectrum is currently retained.

changeably for the Ising model, and that the magnetization per site is approximated, within the CTMRG algorithm, by the expectation value of the central spin. See ??.

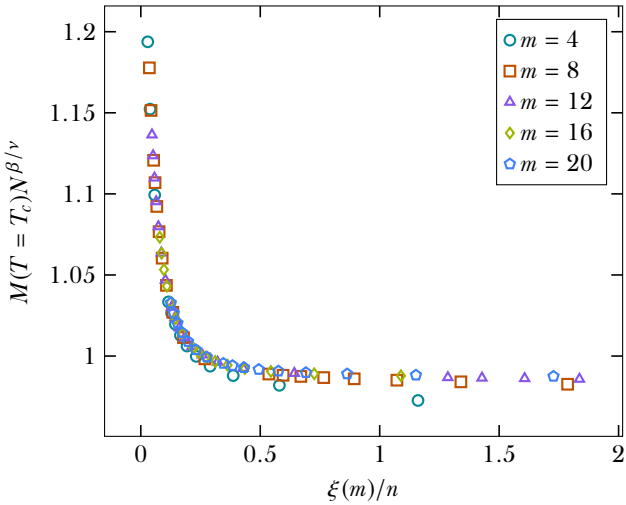

Figure 2.2: Scaling function $\mathcal{G}(\xi(m)/N)$ given in Eq. 2.3.

To further test the hypothesis that N and $\xi(m)$ are the only relevant length scales, the authors of [6] propose a scaling relation for the order parameter M at the critical temperature of the form

$$M(N, m) = N^{-\beta/\nu}\mathcal{G}(\xi(m)/N) \tag{2.3}$$

with

$$\mathcal{G}(x) = \begin{cases} \text{const} & \text{if } x \to \infty, \\ x^{-\beta/\nu} & \text{if } x \to 0, \end{cases} \tag{2.4}$$

meaning that Eq. 2.3 reduces to Eq. 2.2 in the limit $\xi(m) \gg N$ and to Eq. 2.1 in the limit $N \gg \xi(m)$. Fig. 2.2 shows that the scaling relation of Eq. 2.3 is justified.

Fig. 2.3 shows the cross-over behaviour from the N-limiting regime, where $M(N, m) \propto N^{-\beta/\nu}$ to the $\xi(m)$-limiting regime, where $M(N, m)$ does not depend on N.

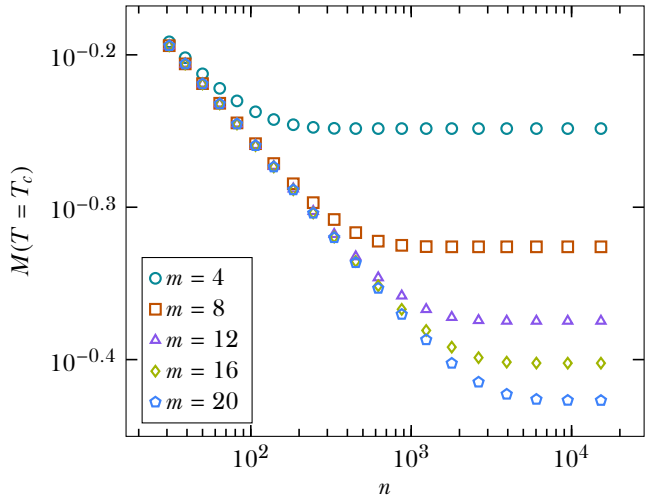

Figure 2.3: Behaviour of the order parameter at fixed m as function of the number of renormalization steps n. For small n, all curves coincide, since the system size is the only limiting length scale. For large enough n, the order parameter is only limited by the length scale $\xi(m)$. In between, there is a cross-over described by $\mathcal{G}(\xi(m)/N)$, given in Eq. 2.3.

2.1.2 Central charge

We may directly verify the value of the central charge c associated with the conformal field theory at the critical point by fitting to

$$S_{\text{classical}} \propto \frac{c}{6} \log \xi(m), \tag{2.5}$$

which yields $c = 0.501$, shown in the left panel of Fig. 2.4.

The right panel of Fig. 2.4 shows the fit to the scaling relation in N (or, equivalently the number of CTMRG steps n)

$$S_{\text{classical}} \propto \frac{c}{6} \log N, \tag{2.6}$$

which yields $c = 0.499$.

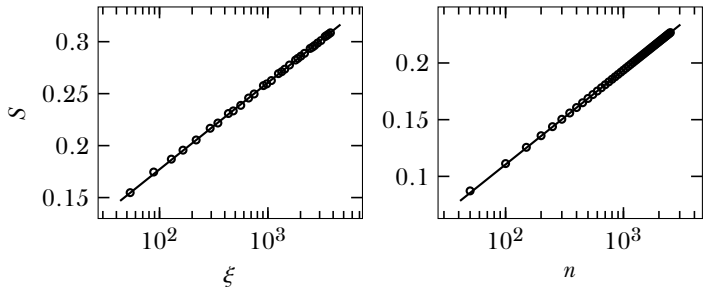

Figure 2.4: Left panel: numerical fit to Eq. 2.5, yielding $c = 0.501$. Here, $m \in \{8, 10, \ldots, 70\}$ and the convergence threshold $\epsilon = 10^{-9}$. Right panel: numerical fit to Eq. 2.6, yielding $c = 0.499$, with the fit made to $n \in \{1500, 1550, \ldots 2500\}$, such that the truncation error is smaller than 10^{-7}.

2.1.3 Using the entropy to define the correlation length

Via ??, the correlation length is expressed as

$$\xi \propto \exp(\frac{6}{c}S). \tag{2.7}$$

Fig. 2.5 shows the results of fitting the relation in Eq. 2.1 with this definition of the correlation length. The fit is an order of magnitude better in the least-squares sense, and the half-moon shapes have almost disappeared, yielding a much more robust exponent of $\beta/\nu = 0.12498$.

The entropy uses all eigenvalues of the corner transfer matrix, making it apparently less prone to structure in the spectrum than the correlation length as defined in ??, which uses only two eigenvalues of the row-to-row transfer matrix. Furthermore, the corner transfer matrix A is kept diagonal in the CTMRG algorithm, so S is much cheaper to compute than ξ.

2.1.4 Exponent κ

We now check the validity of the relation

$$\xi(m) \propto m^{\kappa} \tag{2.8}$$

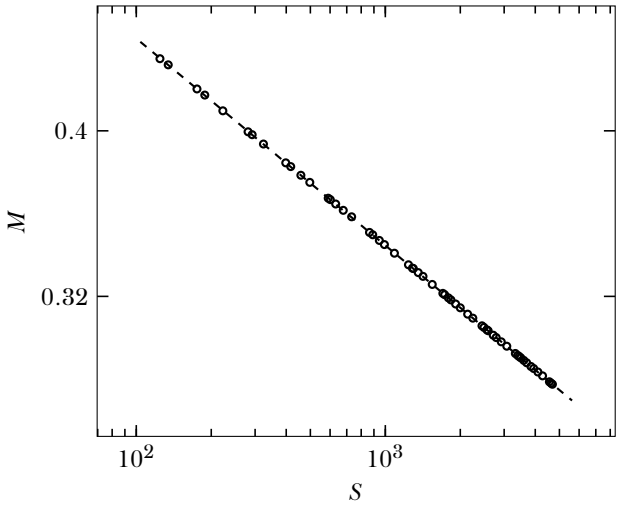

Figure 2.5: Fit to Eq. 2.1, using Eq. 2.7 as the definition of the correlation length. For the fit, we have used $m \in \{10, 11, \ldots, 66\}$, calculated with convergence threshold $\epsilon = 10^{-9}$, yielding $\beta/\nu = 0.12498$.

in the context of the CTMRG method for two-dimensional classical systems. Similar checks were done for one-dimensional quantum systems in [28].

Let us first state that boundary conditions are relevant. From ?? we expect that for fixed boundary conditions, the entropy and therefore the correlation length is lower for a given bond dimension m.

There are various ways of extracting the exponent κ. Fig. 2.6 shows the results for fixed boundary conditions and Fig. 2.7 for free boundary conditions.

Directly checking Eq. 2.8 yields $\kappa = 1.93$ for a fixed boundary and $\kappa = 1.96$ for a free boundary.

Under the assumption of Eq. 2.8, we have the following scaling laws at the

critical point

$$M(m) \propto m^{-\beta\kappa/\nu} \tag{2.9}$$

$$f(m) - f_{\text{exact}} \propto m^{(2-\alpha)\kappa/\nu} \tag{2.10}$$

for the order parameter and the singular part of the free energy, respectively. With a fixed boundary, a fit to $M(m)$ yields $\kappa = 1.93$. For a free boundary we cannot extract any exponent, since $M = 0$ for every temperature. A fit to $f(m) - f_{\text{exact}}$ yields $\kappa = 1.90$ for a fixed boundary and $\kappa = 1.93$ for a free boundary. Fig. 2.6. Here, we have used $\beta = 1/8$, $\nu = 1$ and $\alpha = 0$ for the Ising model.

We may use ?? and ?? to check the relation

$$S_{\text{classical}} \propto \frac{c\kappa}{6} \log m, \tag{2.11}$$

which yields $\kappa = 1.93$ for a fixed boundary and $\kappa = 1.96$ for a free boundary, with $c = 1/2$ for the Ising model.

2.1.4.1 Comparison with exact result in asymptotic limit

The predicted value for κ [29] is 2.034 . . . (see also ??). With the CTMRG method, we extract the slightly lower value of 1.96 (corresponding to free boundary conditions). But, the structure in the quantities as function of m makes it hard to get an accurate fit to κ.

It is interesting to note that for fixed boundary conditions, the relation in Eq. 2.8 holds, but with a lower exponent κ. This is to be expected, since half the spectrum of the corner transfer matrix is missing.

2.2 Locating the critical point

In general, the critical point is not known, but it may be located by extrapolating the position of the pseudocritical temperature at finite system sizes.

The pseudocritical point can be defined in a variety of ways. In this chapter, we will define the pseudocritical point as the point of maximum entropy, as described in ??. Fig. 2.8 shows the classical analogue to the entanglement entropy as a function of temperature for different values of m.

The critical point is located by fitting the scaling law in ??.

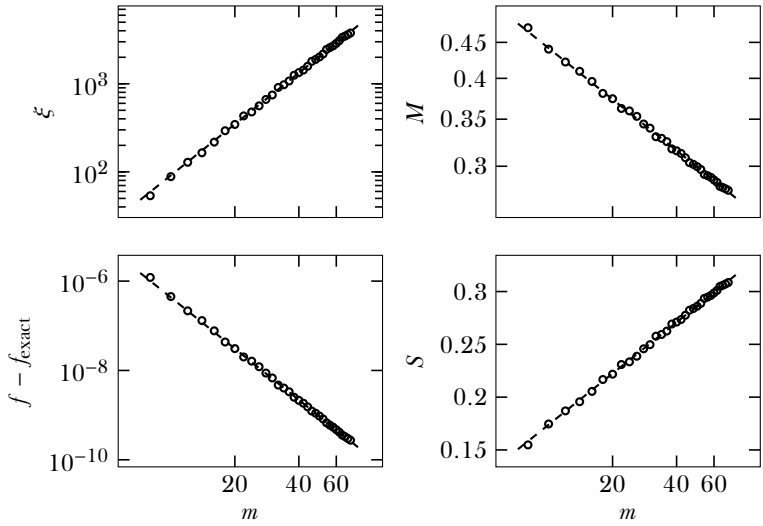

Figure 2.6: Numerical evidence for Eq. 2.8, Eq. 2.9, Eq. 2.11 with fixed boundary, yielding, from left to right and top to bottom, $\kappa = \{1.93, 1.93, 1.90, 1.93\}$. These values have been calculated from simulations with $m \in \{8, 10, \ldots, 70\}$ and convergence threshold $\epsilon = 10^{-9}$.

2.2.1 Finite m

For approximations with finite bond dimension m, we may use different length scales to fit the scaling behaviour of $T^\star(m)$. In light of the discussion in **??**, we can choose either $\xi(T_c, m)$ or $\xi(T^\star(m), m)$. The latter suffers less from finite-size effects, but is dependent on the accuracy with which $T^\star$ is located. It is, of course, of more general interest since T_c is normally not known.

Furthermore, we will consider both $\xi(m)$ derived from the row-to-row transfer matrix (**??**) and derived from the entanglement entropy (Eq. 2.7).

Fig. 2.9 shows the fits for different choices of this length scale. The results are tabulated in Table 2.1. To obtain $T^\star$, we have calculated $T^\star(m)$ for $m \in \{10, 11, \ldots, 60\}$ with a convergence threshold of 10^{-8} and a temperature tolerance of 10^{-8}. The boundaries are fixed to +1.

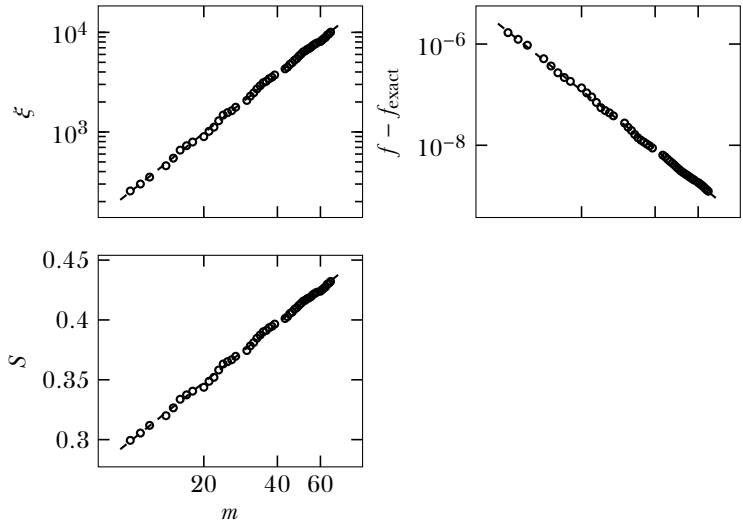

Figure 2.7: Numerical evidence for Eq. 2.8 with free boundary, yielding from left to right and then bottom $\kappa = \{1.96, 1.93, 1.96\}$. These values have been calculated from simulations with $m \in \{10, 11, \ldots, 66\}$, but with $m \in \{13, 19, 28, 29, 40, 41, 42, 59\}$ left out, because for those values m the system breaks its symmetry (see ??). The convergence threshold was chosen to be $\epsilon = 10^{-7}$. It is not feasible to choose a lower threshold since more values of m break symmetry as machine precision is approached.

We denote the estimated value of the critical temperature as $\widetilde{T}_c$. Recall that the exact value is

$$T_c = 2.2691853\ldots \tag{2.12}$$

and

$$\nu = 1. \tag{2.13}$$

When using $\xi(T_c, m)$, the correlation length at the exact critical point, the result shows a lot of structure, yielding $\widetilde{T}_c = 2.269172$ and $\nu = 1.057$.

N_{eff}	T_c	ν
$\xi(T_c, m)$	2.269172	1.057
$\xi(T^\star(m))$	2.269183	1.002
$\exp((6/c)S(T^\star(m))$	2.269183	1.02
m^κ	2.269181	–
N	2.269185	0.98

Table 2.1: Results for fits to the scaling law ?? using different length scales. When using m^κ, $\kappa \approx 1.91$ was found to give the best fit.

If, instead, the correlation length at the estimated pseudocritical temperature $\xi(T^\star(m))$ is used, the data shows less structure and we obtain the much more precise results $\widehat{T_c} = 2.269183$ and $\nu = 1.002$.

Another option is to use the entropy to define the correlation length, via Eq. 2.7, which gave more accurate results than using the transfer matrix definition in section 2.1.3. In this case, the results are slightly worse than the transfer matrix definition: $T_c = 2.269183$ and $\nu = 1.02$.

Finally, we may directly fit the law

$$|T_c - T^\star(m)| \propto m^{-\kappa/\nu}, \tag{2.14}$$

yielding $T_c = 2.269181$ and $\kappa/\nu = 1.91$. Incidentally, this is another way to confirm $\kappa \approx 1.9$ for systems with a fixed boundary.

2.2.2 Finite N

As a cross check, we can instead use systems of finite size to extract T_c and ν. We have calculated $T^\star(n)$ for $n \in \{2300, 2500, \ldots, 7900\}$, with m big enough such that the truncation error is no larger than 10^{-6}. This yields $T_c = 2.269185$ and $\nu = 0.98$.

2.3 Away from the critical point

We may also verify the validity of the different length scales by asserting that the data for different values of m should collapse on a single curve

$$\mathcal{G}(t\xi(m)^{1/\nu}) = M(T, m)\xi(m)^{\beta/\nu}. \tag{2.15}$$

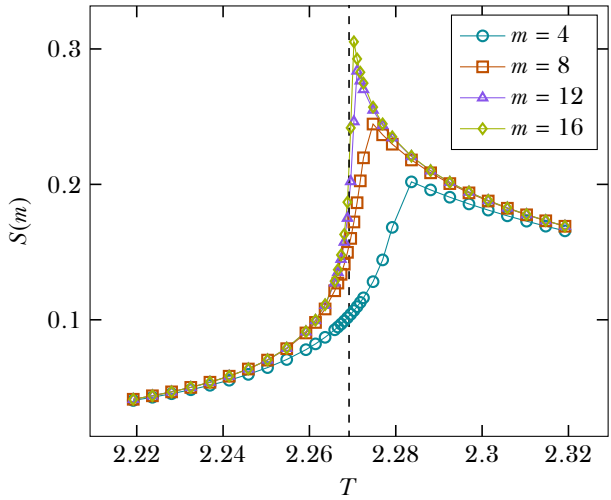

Figure 2.8: Classical analogue to the entanglement entropy, as in ??, near the critical point (shown as dashed line).

All data points were calculated with a convergence threshold of 10^{-7}. The values of the pseudocritical temperatures are taken from the results in section 2.2. No temperatures beyond T_c is considered because the order parameter drops off sharply, causing the curve $\mathcal{G}(x)$ to tend to zero almost vertically, making the fitness P unreliable.

Fig. 2.10 shows that for all length scales, the results more or less fall on one curve. Table 2.2 shows the fitness of the data collapse [30] (given by ??) for all length scales used.

Using m^κ as a length scale for optimized fitness $P(\kappa)$ yields $\kappa \approx 1.98$, substantially higher than found previously for fixed boundary conditions.

As a cross-check, the bottom-right panel of Fig. 2.10 shows data points for finite-N simulations. Here, the bond dimension is chosen such that the truncation error is smaller than 10^{-6}.

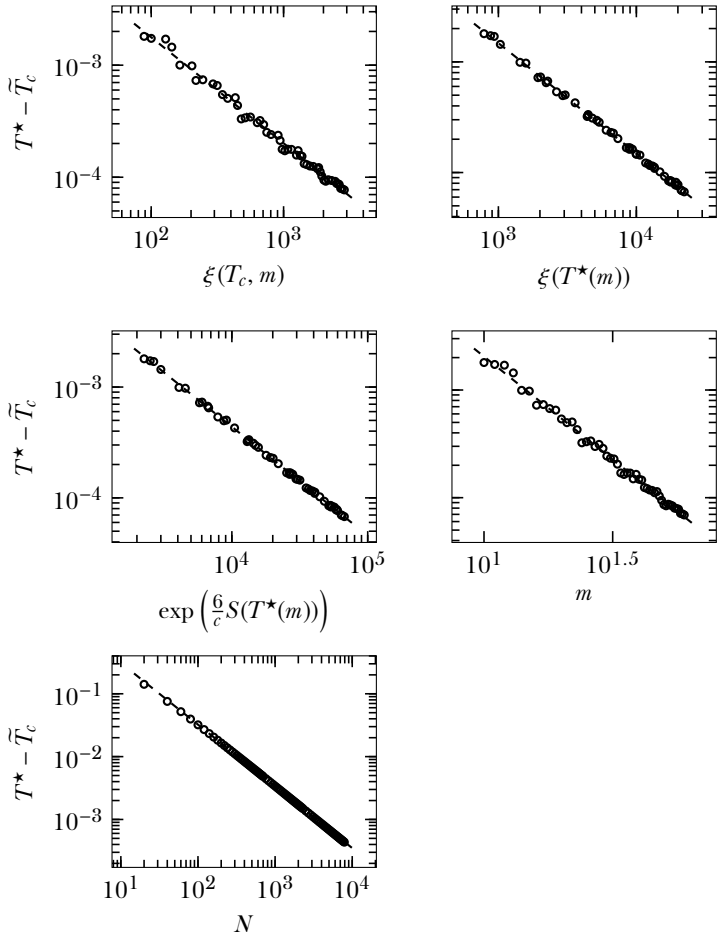

Figure 2.9: Fits to the scaling law ??. Results for the critical temperature and exponent ν are tabulated in Table 2.1.

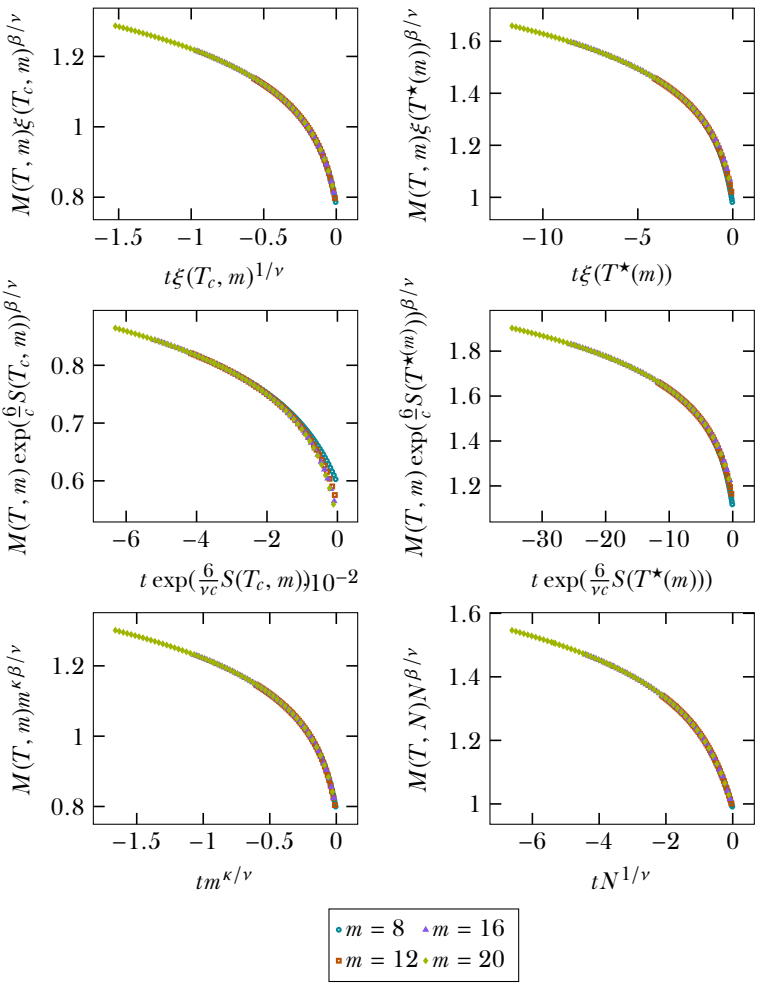

Figure 2.10: Data collapses using different length scales. For the bottom-right plot, approximations with finite N instead of finite m have been used, with $n = \{160, 480, 1000, 1500\}$ ($n = \frac{N-1}{2}$ is the number of algorithm steps).

N_{eff}	fitness P
$\xi(T_c, m)$	0.0075
$\xi(T^\star(m))$	0.066
$\exp((6/c)S(T_c, m))$	0.057
$\exp((6/c)S(T^\star(m))$	0.087
m^κ	0.0080
N	0.0075

Table 2.2: Fitness of data collapse (??) for different length scales. $\kappa \approx 1.98$ was found to be optimal for the length scale m^κ.

2.4 Discussion

2.4.1 Finite-m vs finite-size simulations

With finite-m simulations, larger system sizes are accessible. This is clearly seen from the fact that for modest values of m, $T^\star(m)$ is already closer to the critical point than $T^\star(N)$ for the largest values of N.

For the Ising model, finite-size and finite-m scaling give comparable results. However, finite-size data is of much higher quality than the finite-m data, since the latter suffers from structure due to the spectrum of the corner transfer matrix, even when defining the correlation via the entanglement entropy. Therefore, it is likely that finite-size results improve significantly if correction to scaling terms are included in the fits.

For finite-size simulations, it is not entirely clear how the chosen bond dimension (and correspondingly, the truncation error) influences the precision of quantities and the position of the pseudocritical point. This could be analysed more thoroughly. A start with this has been made in ??.

It might be possible to simulate larger system sizes without much loss of accuracy, but it seems unlikely that the same system sizes as in the finite-m regime are accessible.

For finite-m results it is much easier to assess the convergence of quantities (see ??). The quality of the fit remains limited by the structure that is inherent in the data.

2.4.2 Exponent κ

We consistently find a value for the exponent κ that is between 1.93 and 1.96 (for simulations with free boundary conditions), while the theoretically predicted value is approximately 2.034.

The first reason for this might simply be the fact that the data has half-moon shaped patterns that make it hard to extract an exponent reliably.

A second possibility is that, since the predicted value for κ is only valid in the limit $m \to \infty$, finite-m effects cause the exponent obtained from numerical simulation to be lower. This is confirmed by the authors of [29], who use the iTEBD algorithm [26] to obtain $\kappa = 1.92$ for the Ising model and $\kappa = 1.26$ for the XXZ model (predicted value $1.34\ldots$), among other results. However, the authors of [28] consistently find $\kappa \approx 2$ for the Ising model using iTEBD.

A third possibility is that the corner transfer matrices used for the calculations in this work do not represent optimal matrix-product states. In theory, the CTMRG algorithm should produce an optimized row-to-row transfer matrix with matrix product structure in the thermodynamic limit [2]. But because simulations with free boundary conditions are sensitive to numerical errors, we could only choose a moderately low convergence threshold. This might in part explain the observed discrepancy.

3
Numerical results for the clock model

We present a numerical study of the square-lattice clock model with $q = \{5, 6\}$ states. We employ the corner transfer matrix renormalization group method, working in both finite-size and finite-m regimes.

The model has a low-temperature ordered phase, a massless phase and a high-temperature disordered phase. We locate the transition temperatures T_1 and T_2 by extrapolating the positions of pseudocritical temperatures, assuming the transitions are of the Kosterlitz-Thouless type.

The pseudocritical temperature is defined as the point where the classical analogue of the entanglement entropy reaches its maxixum. For free (fixed) boundary conditions the entropy peaks near T_1 (T_2).

In addition, we calculate the central charge and the magnetization exponent in the massless phase. In comparison with exact results for the Villain formulation, the magnetization exponent suggests that the locations of T_1 and T_2 found in this work might underestimate the extent of the massless phase, but we argue it is plausible that this is due to finite-size effects.

3.1 Introduction

In the field of phase transitions and critical phenomena, the two-dimensional topological phase transition discovered by Kosterlitz and Thouless [31, 32] receives much attention. This phase transition is characterized not by an order parameter which indicates a breaking of symmetry, but by the proliferation of topological defects.

In the low-temperature phase, the two-point correlation functions decay with a power-law with varying exponent $\eta(T)$. At the transition, the correlation length diverges as

$$\xi \propto \exp(A|T - T_c|^{-1/2}), \tag{3.1}$$

with A a non-universal constant. Above the transition, the two-point correlators decay exponentially.

The XY model consists of planar rotors on the square lattice. It exhibits the Kosterlitz-Thouless (KT) phase transition and by the Mermin-Wagner-Hohenberg theorem the symmetry of the ground state is broken for all temperatures, due to the $O(2)$ (planar rotational) symmetry of the potential [33, 34].

The q-state clock model possesses the discrete $\mathbb{Z}_q$ symmetry and is an interpolation between the Ising model, which corresponds to $q = 2$, and the XY model, which corresponds to $q \to \infty$. Its energy function is given by

$$H_q = -\sum_{\langle ij \rangle} \cos(\theta_i - \theta_j), \tag{3.2}$$

with the spins taking the values

$$\theta = \frac{2\pi n}{q} \qquad n \in \{0, \ldots, q-1\}. \tag{3.3}$$

It has been proven that for high enough q, this model indeed exhibits a Kosterlitz-Thouless transition [35]. Furthermore, it has been proven that for $q \geq 5$, a general model with $\mathbb{Z}_q$ symmetry (of which Eq. 3.2 is a special case) has three phases: a symmetry broken phase for $T < T_1$, an intermediate phase with power law decay of the correlation function, and a high-temperature phase with exponential decay of the correlation function for $T > T_2$ [36].

In the Villain formulation of the potential [37], it has been proven that the transition at T_2 is a BK-transition [38], and numerical results suggest that for a broad range of temperatures, the thermodynamic behaviour becomes identical to the XY model for high enough q [39].

Furthermore, in the Villain formulation it is known that [40, 41]

$$\eta(T_1) = \frac{4}{q^2}, \qquad \eta(T_2) = \frac{1}{4}, \tag{3.4}$$

where η is the spin-spin correlation function exponent. In CTMRG simulations, it is possible to obtain this exponent through the relation

$$\frac{\eta}{2} = \frac{\beta}{\nu}, \tag{3.5}$$

where the fraction $\frac{\beta}{\nu}$ is found by finite-size scaling of the magnetization (see ??).

For the cosine model in Eq. 3.2, the value q_c for which it first exhibits a BK-transition is not precisely known. There is some disagreement about whether the cases $q = 5, 6$ exhibit KT-type transitions (see previous numerical results below).

In our simulations we will focus on the cases $q = 5, 6$, to (i) study the nature of the phase transition from the new perspective provided by the corner transfer matrix formalism and (ii) compare the accuracy of finite-m and finite-N scaling within the CTMRG method to other established numerical methods.

We summarise previous numerical results, then present results obtained with the CTMRG algorithm and finish with a discussion.

3.2 Previous numerical results

3.2.1 The $q = 5$ clock model

The general consensus is that the two transitions of the $q = 5$ clock model with cosine potential are of the KT-type, though there are no rigorous results. It is also assumed that the critical indices are the same as those in the Villain formulation.

The disagreement about the nature of the phase transitions stems from numerical results for the helicity modulus [42].

Most notably, Baek and Minnhagen [43] claim that since the helicity modulus does not vanish in the high-temperature phase, the upper transition is not of the KT-type.

It was shown by Kumano et al. in [44], however, that the definition used by Baek and Minnhagen is not suitable for systems with a discrete symmetry. The correct discrete definition yields the expected result, namely that the helicity modulus does vanish and the three-phase KT-picture holds.

The conclusion of Kumano et al, which was obtained by a Monte Carlo study, was verified by Chatelain [45] using the TMRG algorithm [46] (see also ??). Chatelain also found that the critical indices match those of the Villain model (Eq. 3.4), implying the cosine model is in the same universality class.

After the rebuttal by Kumano et al., Baek et al. published another work [47] in which they again use the (in the eyes of Kumano et al.) wrong definition of the helicity modulus, yet calculated in a different way. Again they conclude the transition is not of the KT-type.

Meanwhile, Borisenko et al. [48] carried out a very detailed Monte Carlo study confirming the KT-picture, using Binder-cumulants to find the critical points and the magnetization and susceptability to find the critical indices.

	T_1	T_2
Brito et al.[1] (2010) [49]	0.91	0.90
Borisenko et al. (2011) [48]	0.9056	0.9432
Kumano et al. (2013) [44]	0.908	0.944
Chatelain (2014) [45]	0.914	0.945
This work (finite-N scaling)	0.915	0.935
This work (finite-m scaling)	-	0.944

Table 3.1: Previous results for the transition temperatures for $q = 5$.

Brito et al. [49] conclude from a Monte Carlo study that while the transition is of KT-type, the resolution of their numerical method is not high enough to distinguish between T_1 and T_2.

Table 3.1 shows the results for the transition temperatures found by other authors.

3.2.2 The $q = 6$ clock model

Here, there is overwhelming consensus that both transitions are of the KT-type. The only exceptions are Lapilli et al. [39] and Hwang [50].

Lapilli et al. use the incorrect definition of the helicity modulus.

Hwang asserts that the transition is not of KT-type because the data, which was obtained from systems of rather small size ($L \times L$-systems with $L = 20, \ldots, 28$), also agrees with a power-law divergence of the correlation length.

The previous results for the transition temperatures are listed in Table 3.2. For an overview that goes further back, see [51].

We note that [44, 49, 52] use Monte Carlo methods, while [51] uses the CTMRG algorithm (combined with finite-size scaling, but not with finite-m scaling).

[1] These authors found $T_1 > T_2$, which is not an error in the text, but due to the low resolution of the methods used.

[2] To obtain these values, the author assumed an algebraic divergence of the correlation length.

	T_1	T_2
Tomita and Okabe (2002) [52]	0.7014	0.9008
Hwang[2] (2009) [50]	0.632	0.997
Brito et al. (2010) [49]	0.68	0.90
Kumano et al. (2013) [44]	0.700	0.904
Krčmár et al. (2016) [51]	0.70	0.88
This work (finite-N scaling)	0.700	0.883
This work (finite-m scaling)	-	0.901

Table 3.2: Previous results for the transition temperatures for $q = 6$.

3.3 Spectrum of the corner transfer matrix

In order to get an idea of the accuracy that we might expect, we have plotted the spectrum of the $q = \{5, 6\}$ clock models in Fig. 3.1.

It is clear that the spectra of both clock models fall off at about the same pace, if we compare points in the ordered, massless and disordered phase. The $q = 6$ clock model has a slightly more degenerate spectrum, as might be expected from its larger symmetry group, but there is no clear pattern.

As compared to the Ising model (see ??), the spectra of the $q = \{5, 6\}$ clock models fall off much more slowly[3]. This implies that a much larger bond dimension is needed to obtain the same accuracy for quantities in the thermodynamic limit.

3.4 Magnetization

For the clock model, we define the magnetization per site as

$$M = \langle \cos \theta_0 \rangle, \tag{3.6}$$

where θ_0 is the central spin.

[3]For the calculation of the spectrum of the Ising model in this work, a bond dimension of $m = 250$ was used, as opposed to $m = 100$ for the clock model. This means that, in small part, the slower decay of the spectrum is due to the normalization $\mathrm{Tr}\, A^4 = 1$. But this does not change the general picture that the spectra of the $q = \{5, 6\}$ clock models decay more slowly.

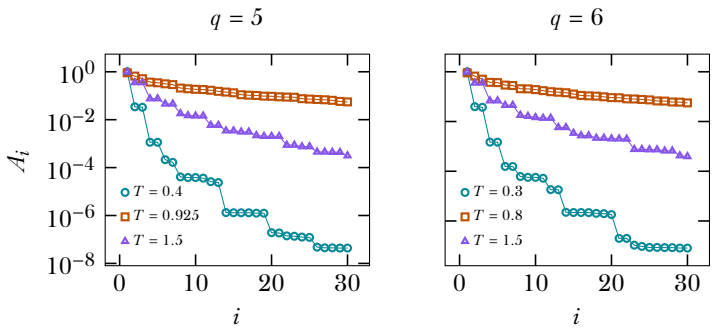

Figure 3.1: First part of the spectrum of A with fixed boundary, calculated with $m = 100$ and a convergence threshold of 10^{-8}, at temperatures corresponding to the ordered phase, approximate midpoint of the massless phase and disordered phase, respectively.

This quantity can be computed in the same way as for the Ising model (see ??) by generalizing the tensor b_{ijkl} to

$$b_{ijkl} = \sum_{n\in\{0,\dots,q-1\}} \cos\left(\frac{2\pi n}{q}\right) \delta_{nijkl}. \tag{3.7}$$

3.5 Classical analogue to the entanglement entropy

The classical analogue to the half-chain entanglement entropy S is defined in ??. Its definition remains valid.

In the limit $T \to \infty$, for both a fixed and free boundary, we have

$$S(T \to \infty) = 0. \tag{3.8}$$

To see this, consider that all 2^{2N} configurations on the inner edges of the $N \times N$ quadrant represented by the corner transfer matrix are equally likely in this limit, hence

$$A_{ij} = \frac{1}{2^{2N}}, \tag{3.9}$$

which has one eigenvalue of 1 and the others 0[4].

In the limit $T \to 0$, there is only one non-zero matrix element in the case of a fixed boundary (namely all inner spins having the same value as the outer boundary), and q equally likely configurations in the case of a free boundary, yielding

$$S^{\text{fixed}}(T = 0) = 0,$$
$$S^{\text{free}}(T = 0) = \log q.$$

For a fixed boundary, the point of maximum entropy approaches the massless phase from the high-temperature region, hence tending towards T_2. In contrast, the point of maximum entropy approaches T_1 for systems with a free boundary.

Fig. 3.2 and Fig. 3.3 show these quantities for $q = 5$ and $q = 6$ for systems with a fixed boundary, clearly confirming the three-phase picture.

3.6 Transition temperatures

Since we expect an essential singularity of the form in Eq. 3.1 for both transitions, for finite systems we have

$$N = a \exp\left(b|T^\star(N) - T_c|^{-1/2}\right), \tag{3.10}$$

where N is an effective finite length scale of the system and a and b are non-universal constants.

N is the system size in the case of finite-size scaling and a length scale derived $\xi(m)$ from the bond dimension m in the case of finite-m scaling. Throughout this chapter, we have defined $\xi(m)$ through the relation

$$S \propto \frac{c}{6} \log \xi(m) \tag{3.11}$$

where $c = 1$ is expected, since the massless phase corresponds to a Gaussian model [32]. These assumptions are validated in section 3.7.1.

We define $T^\star(N)$ as the point of maximum entanglement entropy, as discussed in ??.

[4] One can also make the argument that the corresponding quantum state tends to a product state in the limit $T \to 0$, yielding the same conclusion.

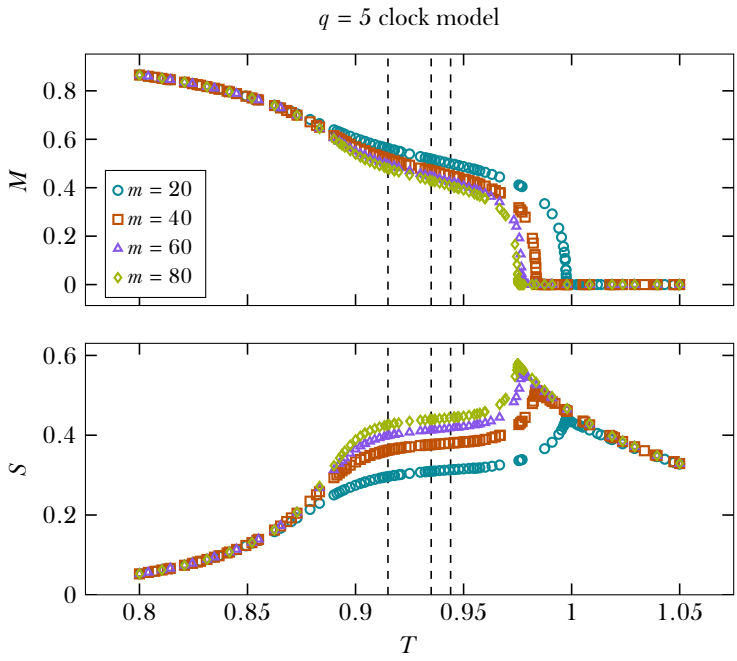

Figure 3.2: Classical analogue to half chain entanglement entropy (??) and magnetization (Eq. 3.6) computed for systems with a fixed boundary for the $q = 5$ clock model. Simulations were done with a convergence threshold of 10^{-7}. The dashed lines denote the transition temperatures found in this study.

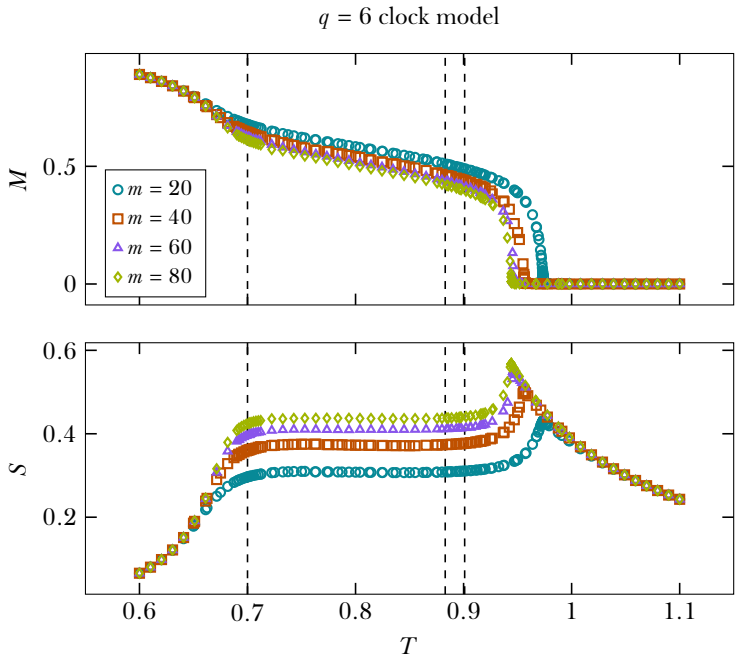

Figure 3.3: Classical analogue to half chain entanglement entropy (??) and magnetization (Eq. 3.6) computed for systems with a fixed boundary for the $q = 6$ clock model. Simulations were done with a convergence threshold of 10^{-7}. The dashed lines denote the transition temperatures found in this study.

Inverting Eq. 3.10 gives the following relations for the pseudocritical transition temperatures

$$T_1^\star(N) = -\frac{\alpha_1}{(\log \beta_1 N)^2} + T_1 \tag{3.12}$$

$$T_2^\star(N) = \frac{\alpha_2}{(\log \beta_2 N)^2} + T_2 \tag{3.13}$$

where $\alpha = b^2$ and $\beta = 1/a$ (we drop the subscripts denoting the transition).

For convenience, we define the scaled length variable

$$\ell = (\log \beta N)^2, \tag{3.14}$$

such that

$$T^\star(N) - T_c \propto \frac{1}{\ell}. \tag{3.15}$$

3.6.1 Numerical difficulties with finite-m simulations around T_1

For both the $q = \{5, 6\}$ clock models, it has been found that locating $T_1^\star(m)$ is not possible, since for systems with a free boundary, numerical errors cause the matrices A and P to lose their symmetry and converge to a fixed boundary fixed point instead. This happens after a modest amount of steps, especially near $T_1(m)^\star$, making it impossible to reach any feasible convergence threshold such as 10^{-6}.

This means that for locating T_1, we must rely on finite-size scaling, whereas for locating T_2 we can rely on both finite-size and finite-m scaling.

3.6.2 Transition from the ordered to the massless phase T_1

Fig. 3.4 and Fig. 3.5 show the fits to Eq. 3.10 for $q = \{5, 6\}$, yielding

$$T_1^{q=5} = 0.915, \qquad T_1^{q=6} = 0.700. \tag{3.16}$$

Conform to the Kosterlitz-Thouless divergence of the correlation length, the pseudocritical temperatures indeed become linear in $\frac{1}{\ell}$, with ℓ defined in Eq. 3.14.

It is interesting to note that finite-size effects are much more pronounced for $q = 5$.

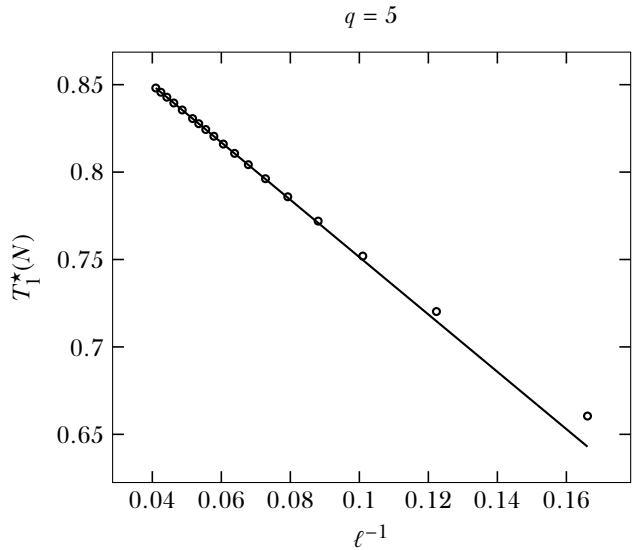

Figure 3.4: We find $T_1 = 0.915$ for the $q = 5$ clock model. We have fitted the final 8 points $n = \{60, 65, 70, 80, 90, 100, 110, 120\}$. Not included in the fit are $n = \{10, 15, \ldots, 55\}$. m was chosen such that the truncation error was smaller than 10^{-6} for $n \leq 70$ and smaller than 10^{-5} for $n > 70$. In finding the maximum of the entropy, a tolerance in temperature of 10^{-5} was used.

3.6.3 Transition from the massless to the disordered phase T_2

3.6.3.1 Finite-size scaling

Finite-size scaling, shown in Fig. 3.6 for $q = 5$ and Fig. 3.8 for $q = 6$ yields

$$T_2^{q=5} = 0.935, \qquad T_2^{q=6} = 0.883. \tag{3.17}$$

For both clock models, finite-size effects are large. For $q = 6$, the finite-size effects are more pronounced than at T_1.

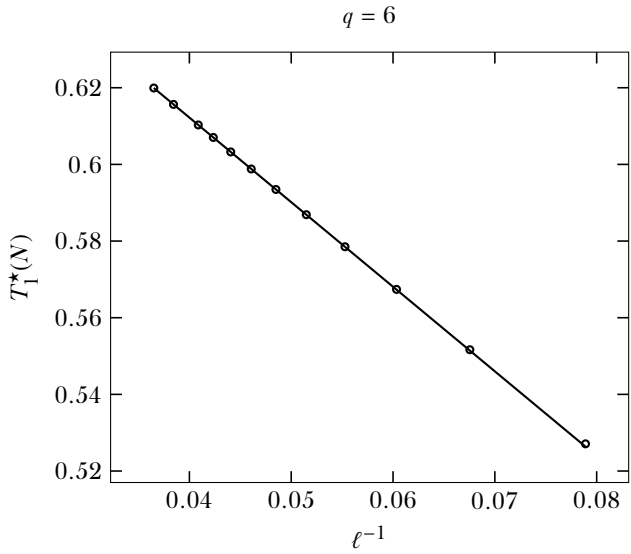

Figure 3.5: We find $T_1 = 0.700$ for the $q = 6$ clock model. We have fitted the final 8 points $n = \{35, 40, 45, 50, 55, 60, 70, 80\}$. Not included in the fit are $n = \{15, 20, 25, 30\}$. m was chosen such that the truncation error was smaller than 10^{-6} for $n \leq 60$ and smaller than 10^{-5} for $n > 60$. In finding the maximum of the entropy, a tolerance in temperature of 10^{-5} was used.

3.6.3.2 Finite-m scaling

Finite-m scaling, shown in Fig. 3.10 for $q = 5$ and Fig. 3.9 for $q = 6$ yields

$$T_2^{q=5} = 0.944, \qquad T_2^{q=6} = 0.901. \tag{3.18}$$

It is seen that with finite-m simulations, systems of significantly larger effective size can be simulated. From the finite-size fits to $T_2^\star(N)$, it can be estimated that a system of $m = 90$ approximately corresponds to a 2700×2700 lattice for $q = 5$ and a 2400×2400 lattice for $q = 6$.

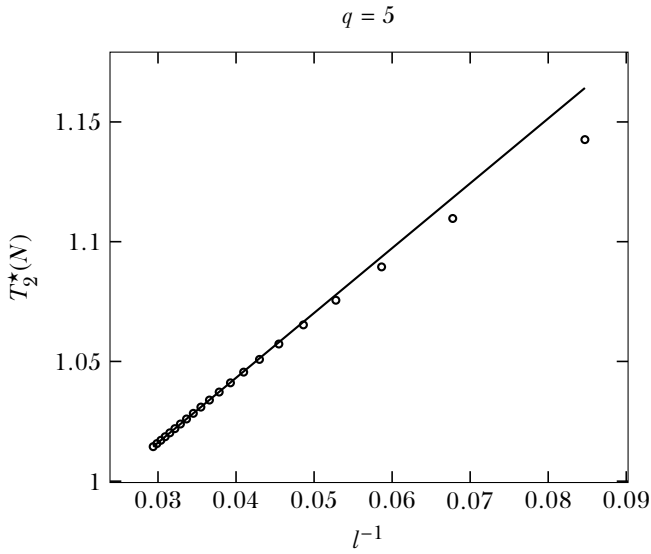

Figure 3.6: We find $T_2 = 0.935$ for the $q = 5$ clock model with finite-size scaling. We have fitted the final 6 points $n = \{85, 90, \ldots, 110\}$. m was chosen such that the truncation error was smaller than 10^{-6}. In finding the maximum of the entropy, a tolerance in temperature of 10^{-6} was used.

There is some structure in the data, but as long as a wide range of m values is included, the estimation of T_2 is robust.

3.7 The massless phase

3.7.1 Central charge

By fitting the relation in Eq. 3.11, where $\xi(m)$ is calculated as in ??, we can directly extract the central charge of the massless phase.

For $q = \{5, 6\}$ the results are shown in the top panels of Fig. 3.11 and Fig. 3.12. For both models, we recover $c = 1$.

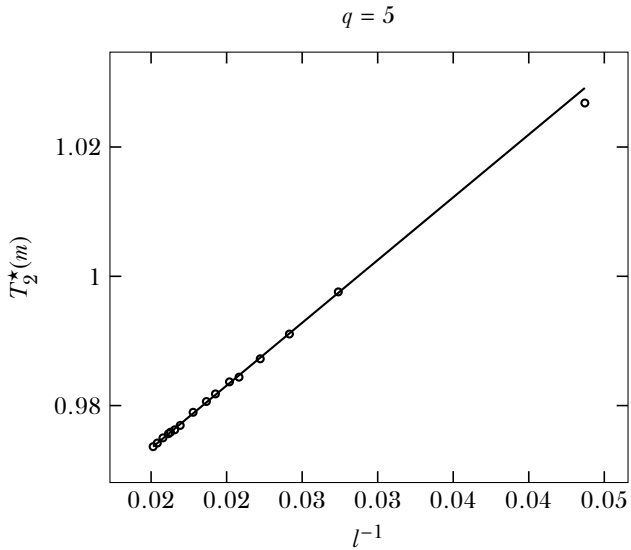

Figure 3.7: For the finite-m simulations, the fit yields $T_2 = 0.944.$ using $m = 20, 25, \ldots, 90$ with a convergence threshold of 10^{-7}. The pseudocritical temperature belonging to $m = 10$ is also shown, but is not included in the fit.

For $q = 5$, the positions of T_1 and T_2 do not precisely agree with the region in which a good fit to Eq. 3.11 can be obtained. The actual massless phase seems to be larger than what the critical temperatures indicate.

However, it is not clear how an effective value of c diverges from 1 outside the massless phase, so we do not draw any conclusions about the correctness of T_1 and T_2 for $q = 5$ based on these results.

3.7.2 Varying exponent for the magnetization

We may verify the exponent with which the magnetization goes to zero in the massless phase by fitting

$$M(m, T) = \xi(m)^{-\frac{\eta(T)}{2}}, \tag{3.19}$$

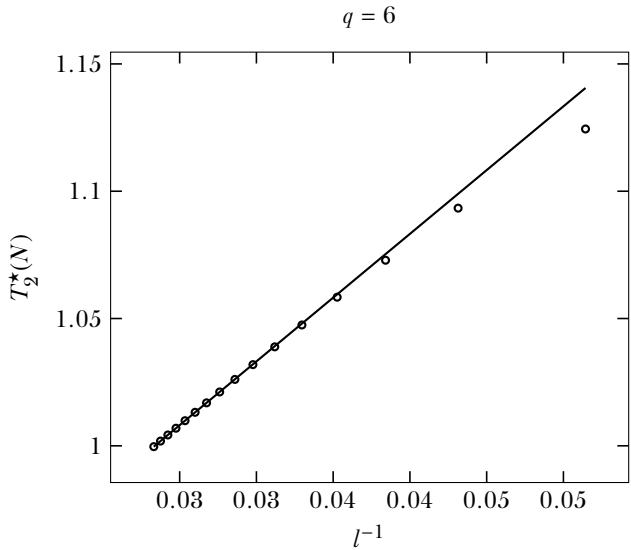

Figure 3.8: We find $T_2 = 0.883$ for the $q = 6$ clock model with finite-size scaling. We have fitted the final 6 points $n = \{60, 65, \ldots, 85\}$. The points $n = \{10, 15, \ldots, 55\}$ were not included. m was chosen such that the truncation error was smaller than 10^{-6}. In finding the maximum of the entropy, a tolerance in temperature of 10^{-6} was used.

with $\xi(m)$ again defined via Eq. 3.11.

The result is shown in the middle panels of Fig. 3.11 and Fig. 3.12 for $q = \{5, 6\}$, respectively.

If we assume that the model under study is in the same universality class as the Villain formulation, η should take the values listed in Eq. 3.4 at the critical points. Again, the positions of the critical points found in this work seem to be too close together, except for the lower transition of $q = 6$, which agrees well with the theoretical value.

Since the lower transition for $q = 6$ suffers the least from finite-size effects, it is plausible that the disagreement between the other transitions and the value

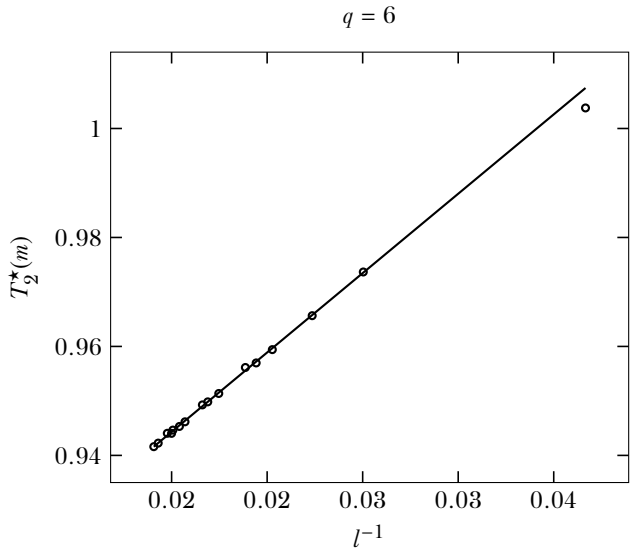

Figure 3.9: For the finite-m simulations, the fit yields $T_2 = 0.901.$ using $m = 20, 25, \ldots, 90$ with a convergence threshold of 10^{-7}. The pseudocritical temperature belonging to $m = 10$ is also shown, but is not included in the fit.

of η will be resolved when larger systems are considered, or finite-size effects are properly taken into account. We come back to this point in the discussion.

The lower panels of Fig. 3.11 and Fig. 3.12 show the norm of residuals of the fit to Eq. 3.19. For $q = 6$, there were values of the magnetization for $0.7 < T < 0.83$ that were lower than expected for certain values of m, reflected by the higher norm of residuals in this region. This did not significantly influence the values of c and η found.

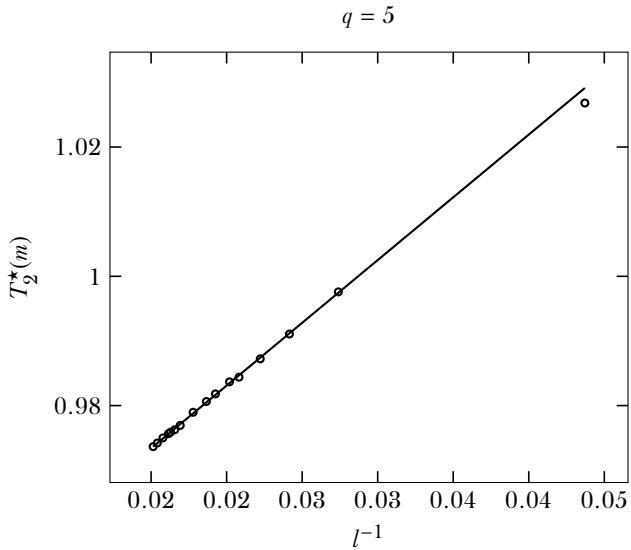

Figure 3.10: For the finite-m simulations, the fit yields $T_2 = 0.944.$ using $m = 20, 25, \ldots, 90$ with a convergence threshold of 10^{-7}. The pseudocritical temperature belonging to $m = 10$ is also shown, but is not included in the fit.

3.8 Discussion

3.8.1 Finite-size effects

Overall, the values of T_1 and T_2 for $q = \{5, 6\}$ in this work agree reasonable well with the values found by other authors, see Table 3.1 and Table 3.2.

Finite-size scaling within the CTMRG suffers more from finite-size effects than finite-m scaling does, since with finite-size simulations smaller system sizes can be reached.

It is plausible that this is the reason that finite-size scaling yields values of the critical temperatures that differ somewhat from previous results and the results of finite-m scaling.

The discussion in section 2.4.1 for the Ising model is applicable here as

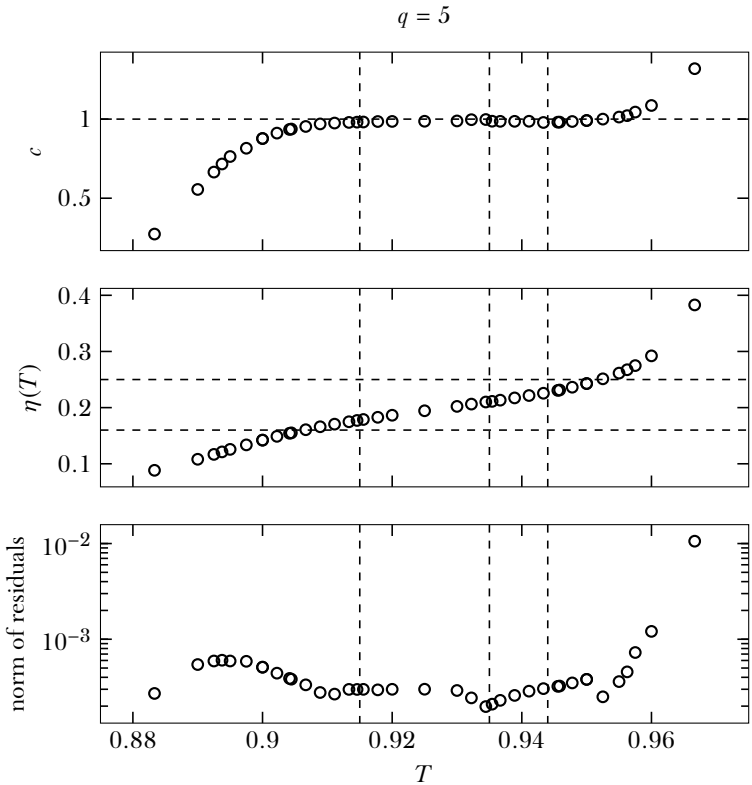

Figure 3.11: Top panel: central charge obtained from fit to Eq. 3.11. The horizontal dashed line marks $c = 1$. Middle panel: $\eta = 2\beta/\nu$ obtained from fit to Eq. 3.19. First 4 values were left out of the fit. The horizontal dashed lines mark $\eta = 4/25$ and $\eta = 1/4$, the exact values obtained in the Villain formulation. Bottom panel: norm of residuals for the fit to Eq. 3.19. For all calculations, we have used $m = 10, 20, \ldots, 100$, simulated with a convergence threshold of 5×10^{-8}. The first four values of m were left out of the fits to mitigate finite-size effects. The vertical dashed lines mark the values of the critical points found in this work, where both results of T_2 are included.

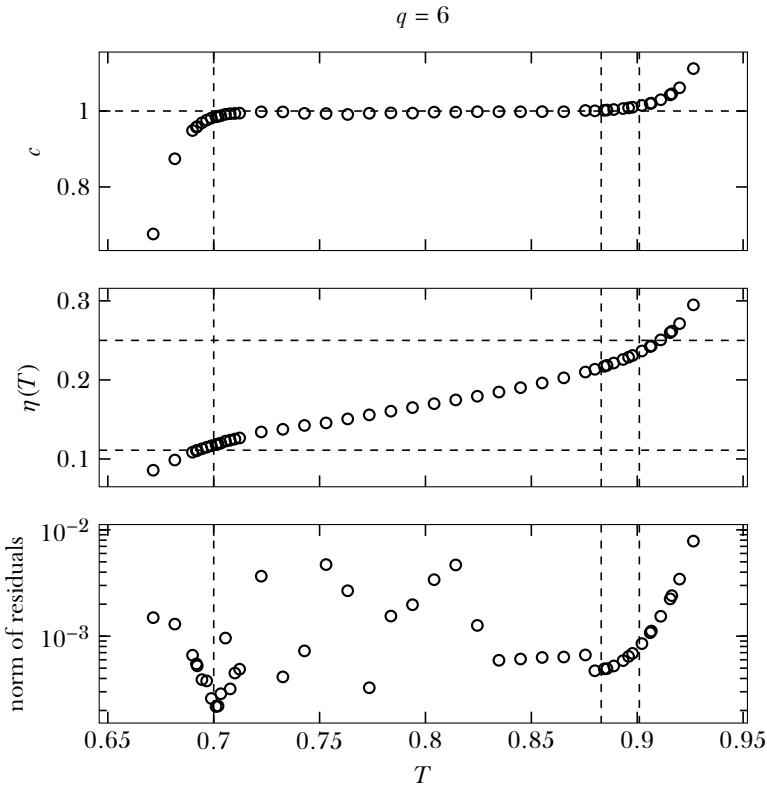

Figure 3.12: Same as Fig. 3.11, except that in the middle panel, the horizontal lines mark $\eta = 4/36$ and $\eta = 1/4$. Finite-size effects were less prominent, but there were some anomalous simulations for $0.7 < T < 0.83$ that showed lower magnetization than expected for certain m-values. We have found that including every m-value in the fit gave the best results.

well. In summary, the most straightforward way of improving finite-size results is to include finite-size corrections, which should be feasible since the data is of high quality. In conjunction with this, a more systematic study of the convergence of quantities and the location of the pseudocritical points (extending results in ??) may reveal that simulating larger system sizes is in fact possible without too much loss of accuracy.

For finite-m scaling, inherent deviations from the basic scaling laws, stemming from the underlying CTM spectrum, make including finite-size corrections less feasible. Using m-values that are far apart or that are specifically selected to mitigate the effects of the half-moon patterns may yield better results.

Results for the exponent η indicate that the critical temperatures found in both this study and previous work might be too close together. It is conceivable that, after considering larger systems and taking into account finite-size corrections, both critical temperatures and the values of η will be adjusted outwards towards their true values, thereby completely reconciling the results.

3.8.2 Other means of studying the transitions T_1 and T_2

In this study, we have used the point of maximum entanglement entropy as a definition of the pseudocritical point. The most obvious drawback of this method is that locating T_1 is not possible with finite-m simulations, as described in section 3.6.1. Finite-size simulations near T_1 are possible, but costly, since the spectrum of the corner transfer matrix decays slowly for systems with a free boundary.

A different way of finding T_1 is through the higher order parameters

$$M_a = \langle e^{ia\theta_0} \rangle, \tag{3.20}$$

which should obey

$$|M_a| \propto \exp\left(-Ca^2/(T_1 - T)^{1/2}\right), \tag{3.21}$$

with C a non-universal constant [36].

M_a is readily obtainable with the CTMRG method and does not require a free boundary. However, it is not clear if this will increase the precision of T_1.

The transition T_2 may also be found by studying the magnetic susceptibility, as was done by [48]. The susceptibility diverges more strongly than the entropy, but requires numerical derivatives to find. It is plausible that this

method would not yield a better accuracy than current method, since it requires the same simulations to obtain T_2. Nonetheless, it would serve as a good consistency check.

Finally, we note that it is possible to introduce the spin-flip symmetry of the Hamiltonian on the tensor level, demonstrated in [53] for the two-dimensional quantum case. This would allow for the studying of T_1 with finite-m approximations.

4
Conclusions

Lorem ipsum dolor sit amet, consectetur adipisicing elit, sed do eiusmod tempor incididunt ut labore et dolore magna aliqua. Ut enim ad minim veniam, quis nostrud exercitation ullamco laboris nisi ut aliquip ex ea commodo consequat. Duis aute irure dolor in reprehenderit in voluptate velit esse cillum dolore eu fugiat nulla pariatur. Excepteur sint occaecat cupidatat non proident, sunt in culpa qui officia deserunt mollit anim id est laborum.

4.1 Outlook

Lorem ipsum dolor sit amet, consectetur adipisicing elit, sed do eiusmod tempor incididunt ut labore et dolore magna aliqua. Ut enim ad minim veniam, quis nostrud exercitation ullamco laboris nisi ut aliquip ex ea commodo consequat. Duis aute irure dolor in reprehenderit in voluptate velit esse cillum dolore eu fugiat nulla pariatur. Excepteur sint occaecat cupidatat non proident, sunt in culpa qui officia deserunt mollit anim id est laborum.

Bibliography

[1] R. J. Baxter, "Variational approximations for square lattice models in statistical mechanics", Journal of Statistical Physics **19**, 461–478 (1978).

[2] R. J. Baxter, *Exactly solved models in statistical mechanics* (Elsevier, 1982) Chap. 13.

[3] S. K. Tsang, "Square lattice variational approximations applied to the Ising model", Journal of Statistical Physics **20**, 95–114 (1979).

[4] T. Nishino, and K. Okunishi, "Corner transfer matrix renormalization group method", Journal of the Physical Society of Japan **65**, 891–894 (1996).

[5] S. R. White, "Density matrix formulation for quantum renormalization groups", Physical Review Letters **69**, 2863 (1992).

[6] T. Nishino, K. Okunishi, and M. Kikuchi, "Numerical renormalization group at criticality", Physics Letters A **213**, 69–72 (1996).

[7] L. P. Kadanoff, "More is the same; phase transitions and mean field theories", Journal of Statistical Physics **137**, 777 (2009).

[8] C. Domb, *The critical point: a historical introduction to the modern theory of critical phenomena* (CRC Press, 1996).

[9] R. Peierls, "On Ising's model of ferromagnetism", Mathematical Proceedings of the Cambridge Philosophical Society **32**, 477–481 (1936).

[10] L. Onsager, "Crystal statistics. I. a two-dimensional model with an order-disorder transition", Phys. Rev. **65**, 117–149 (1944).

[11] T. H. Berlin, and M. Kac, "The spherical model of a ferromagnet", Physical Review **86**, 821–835 (1952).

[12] B. Sutherland, C. N. Yang, and C. P. Yang, "Exact solution of a model of two-dimensional ferroelectrics in an arbitrary external electric field", Physical Review Letters **19**, 588–591 (1967).

[13] R. J. Baxter, "Eight-vertex model in lattice statistics", Physical Review Letters **26**, 832–833 (1971).

[14] R. J. Baxter, *Exactly solved models in statistical mechanics* (Elsevier, 1982).

[15] H. A. Kramers, and G. H. Wannier, "Statistics of the two-dimensional ferromagnet. part ii", Phys. Rev. **60**, 263–276 (1941).

[16] R. B. Griffiths, "Dependence of critical indices on a parameter", Physical Review Letters **24**, 1479–1482 (1970).

[17] M. E. Fisher, "Quantum corrections to critical-point behavior", Physical Review Letters **16**, 11–14 (1966).

[18] R. J. Baxter, "Dimers on a rectangular lattice", Journal of Mathematical Physics **9**, 650–654 (1968).

[19] S. Östlund, and S. Rommer, "Thermodynamic limit of density matrix renormalization", Physical Review Letters **75**, 3537 (1995).

[20] S. Rommer, and S. Östlund, "Class of ansatz wave functions for one-dimensional spin systems and their relation to the density matrix renormalization group", Physical Review B **55**, 2164 (1997).

[21] M. P. Nightingale, and H. W. J. Blöte, "Gap of the linear spin-1 Heisenberg antiferromagnet: a Monte Carlo calculation", Physical Review B **33**, 659–661 (1986).

[22] P. Calabrese, and J. Cardy, "Entanglement entropy and quantum field theory", Journal of Statistical Mechanics: Theory and Experiment **2004**, P06002 (2004).

[23] R. Orús, "A practical introduction to tensor networks: matrix product states and projected entangled pair states", Annals of Physics **349**, 117–158 (2014).

[24] G. Vidal, "Entanglement renormalization", Physical Review Letters **99**, 220405 (2007).

[25] F. Verstraete, and J. I. Cirac, "Renormalization algorithms for quantum-many body systems in two and higher dimensions", arXiv cond-mat/0407066 (2004).

[26] G. Vidal, "Classical simulation of infinite-size quantum lattice systems in one spatial dimension", Physical Review Letters **98**, 070201 (2007).

[27] J. Jordan, R. Orús, G. Vidal, F. Verstraete, and J. I. Cirac, "Classical simulation of infinite-size quantum lattice systems in two spatial dimensions", Physical Review Letters **101**, 250602 (2008).

[28] L. Tagliacozzo, T. R. De Oliveira, S. Iblisdir, and J. I. Latorre, "Scaling of entanglement support for matrix product states", Physical Review B **78**, 024410 (2008).

[29] F. Pollmann, S. Mukerjee, A. M. Turner, and J. E. Moore, "Theory of finite-entanglement scaling at one-dimensional quantum critical points", Physical Review Letters **102**, 255701 (2009).

[30] S. M. Bhattacharjee, and F. Seno, "A measure of data collapse for scaling", Journal of Physics A: Mathematical and General **34**, 6375 (2001).

[31] J. M. Kosterlitz, and D. J. Thouless, "Ordering, metastability and phase transitions in two-dimensional systems", Journal of Physics C: Solid State Physics **6**, 1181 (1973).

[32] J. M. Kosterlitz, "The critical properties of the two-dimensional xy model", Journal of Physics C: Solid State Physics **7**, 1046 (1974).

[33] N. D. Mermin, and H. Wagner, "Absence of ferromagnetism or antiferromagnetism in one-or two-dimensional isotropic Heisenberg models", Physical Review Letters **17**, 1133 (1966).

[34] P. C. Hohenberg, "Existence of long-range order in one and two dimensions", Physical Review **158**, 383 (1967).

[35] J. Fröhlich, and T. Spencer, "The Kosterlitz-Thouless transition in two-dimensional abelian spin systems and the Coulomb gas", Communications in Mathematical Physics **81**, 527–602 (1981).

[36] J. Cardy, "General discrete planar models in two dimensions: duality properties and phase diagrams", Journal of Physics A: Mathematical and General **13**, 1507 (1980).

[37] J. Villain, "Theory of one-and two-dimensional magnets with an easy magnetization plane. II. the planar, classical, two-dimensional magnet", Journal de Physique **36**, 581–590 (1975).

[38] J. V. José, L. P. Kadanoff, S. Kirkpatrick, and D. R. Nelson, "Renormalization, vortices, and symmetry-breaking perturbations in the two-dimensional planar model", Physical Review B **16**, 1217 (1977).

[39] C. M. Lapilli, P. Pfeifer, and C. Wexler, "Universality away from critical points in two-dimensional phase transitions", Physical Review Letters **96**, 140603 (2006).

[40] S. Elitzur, R. B. Pearson, and J. Shigemitsu, "Phase structure of discrete abelian spin and gauge systems", Physical Review D **19**, 3698–3714 (1979).

[41] B. Nienhuis, "Critical behavior of two-dimensional spin models and charge asymmetry in the Coulomb gas", Journal of Statistical Physics **34**, 731–761 (1984).

[42] M. E. Fisher, M. N. Barber, and D. Jasnow, "Helicity modulus, superfluidity, and scaling in isotropic systems", Physical Review A **8**, 1111–1124 (1973).

[43] S. K. Baek, and P. Minnhagen, "Non-Kosterlitz-Thouless transitions for the q-state clock models", Physical Review E **82**, 031102 (2010).

[44] Y. Kumano, K. Hukushima, Y. Tomita, and M. Oshikawa, "Response to a twist in systems with Z_p symmetry: the two-dimensional p-state clock model", Physical Review B **88**, 104427 (2013).

[45] C. Chatelain, "DMRG study of the Berezinskii–Kosterlitz–Thouless transitions of the 2D five-state clock model", Journal of Statistical Mechanics: Theory and Experiment **2014**, P11022 (2014).

[46] T. Nishino, "Density matrix renormalization group method for 2D classical models", Journal of the Physical Society of Japan **64**, 3598–3601 (1995).

[47] S. K. Baek, H. Mäkelä, P. Minnhagen, and B. J. Kim, "Residual discrete symmetry of the five-state clock model", Physical Review E **88**, 012125 (2013).

[48] O. Borisenko, G. Cortese, R. Fiore, M. Gravina, and A. Papa, "Numerical study of the phase transitions in the two-dimensional $Z(5)$ vector model", Physical Review E **83**, 041120 (2011).

[49] A. F. Brito, J. A. Redinz, and J. A. Plascak, "Two-dimensional XY and clock models studied via the dynamics generated by rough surfaces", Physical Review E **81**, 031130 (2010).

[50] C.-O. Hwang, "Six-state clock model on the square lattice: Fisher zero approach with Wang-Landau sampling", Physical Review E **80**, 042103 (2009).

[51] R. Krčmár, A. Gendiar, and T. Nishino, "Phase transition of the six-state clock model observed from the entanglement entropy", arXiv:1612.07611 (2016).

[52] Y. Tomita, and Y. Okabe, "Probability-changing cluster algorithm for two-dimensional XY and clock models", Physical Review B **65**, 184405 (2002).

[53] B. Bauer, P. Corboz, R. Orús, and M. Troyer, "Implementing global abelian symmetries in projected entangled-pair state algorithms", Physical Review B **83**, 125106 (2011).